Design, Modeling and Validation of a Tendon-Driven Soft Continuum Robot for Planar Motion Based on Variable Stiffness Structures

Wilhelm R. Wockenfuß, Viktor Brandt, Linda Weisheit, and Welf-Guntram Drossel

***Abstract*—Robotic structures based on variable stiffness enable high-performance and flexible motion systems that are inherently safe and thus allow safe Human-Robot Collaboration. This letter presents the design of a robotic structure based on variable stiffness. A robotic manipulator is developed using three variable stiff segments based on particle jamming with a backbone architecture and two tendons for an underactuated motion control of the whole structure. By switching the structural stiffness, the manipulator is able to perform complex planar motion with only one pair of tendons, reducing the number of actuators required. A kinematic modeling approach for the calculation of the forward kinematics of this soft continuum structure is presented, and the validation on the real system is explained. The kinematic simulation is performed with a multibody simulation model (MBS) using rigid body elements in combination with rotational springs. The validation of the model is carried out with visual measurements of the real system using defined target shapes. Simulation and experimental results are discussed and compared also with a common constant curvature model. The developed MBS-model demonstrates a promising modeling approach with a position error lower 3% for the calculation of the presented manipulator under gravity.**

***Index Terms*—Soft robot materials and design, compliant joints and mechanisms, modeling, control, and learning for soft robots, tendon/wire mechanism, kinematics.**

I. Introduction

MULTI-SEGMENTED soft continuum robots, unlike conventional rigid-link robots, are characterized by a continuous deformation, compliant structures and thus high dexterity and flexibility. These features make them suitable for human-robot collaboration (HRC) or minimal invasive surgeries (MIS). The design of soft robots is widely researched but they mostly lack stability and stiffness [1], [2]. To combine the advantages of flexible and inherently safe soft robots in terms of HRC and stiffer continuum robots for a better load bearing capability, many studies have been conducted on building variable stiffness robotic structures [3], [4]. But the accurate as well as efficient modeling and control of such robotic structures is difficult. This article shows the design of a robot structure consisting of 3 segments with variable stiffness, which can adjust different planar shapes with different complexity using only 2 tendon actuators, and presents a first approach of a kinematic model to calculate them considering the stiffness variation.

Beside thermal, electrical and magnetically approaches a common way to achieve a variable stiffness is jamming, where particles or layers are enclosed in a flexible and airtight sealed covering [5]. In soft state the particles can nearly free flow and layers can glide above each other. By releasing the air from the inside with a vacuum pump, the particles or layers got tightly packed and got connected via friction force. This approach enables high stiffness ratios ($K > 100$), short switching times ($t < 1$ s) and minimal shape and volume changes between soft and stiff state [6], [7].

In combination with a tendon driven motion control, a multi segmented variable stiff robot based on particle jamming can be built [6]. Other actuator principles for robots with variable stiffness are pneumatic actors [8] like Flexible-Fluid-Actuators [9] or pneumatic chambers used in [10]. Tendon pairs connected with each segment are widespread for enabling the independent motion of the segments [11], [12].

However, most of these approaches require a large number of actuators for complex motion adaptation. The use of structural components with variable stiffness, on the other hand, offers the possibility of realizing a wide variety of shapes with a significantly smaller number of actuators. These are referred to as underactuated mechanisms. This approach has already been used, among others, in the development of soft grippers [13], [14] and enabled the reduction of the required actuators for a uniform gripping motion. By combining this approach with structural elements with variable stiffness, it will now be shown that complex shape adjustments, as required for motion systems, are also possible with underactuated structures.

Correct and accurate modeling of continuum robots is challenging due to the large deformations and coupled influence of external loading, own weight, and actuation on the bending

Manuscript received September 9, 2021; accepted January 5, 2022. Date of publication February 7, 2022; date of current version February 18, 2022. This letter was recommended for publication by Associate Editor G. Palli and Editor C. Gosselin upon evaluation of the reviewers' comments. This work was supported by "Fraunhofer Cluster of Excellence Programmable Materials CPM" for the development of the soft continuum robotic structure. The Modeling and Validation of the Tendon-driven Soft Continuum Robotic Motion Concept was done as part of the cooperation project "BioiC - Bioinspired soft robotic systems for cognitive production" which is being carried out by the University of Naples Federico II and the Fraunhofer Institute for Machine Tools and Forming Technology. Website: https://www.bioic.unina.it/. *(Corresponding author: Wilhelm R. Wockenfuß.)*

The authors are with the Fraunhofer Institute for Machine Tools and Forming Technology, IWU, 01187 Dresden, Germany (e-mail: wilhelm.richard.wockenfuss@iwu.fraunhofer.de; viktor.brandt@iwu.fraunhofer.de; linda.weisheit@iwu.fraunhofer.de; welf-guntram.drossel@iwu.fraunhofer.de).

This letter has supplementary downloadable material available at https://doi.org/10.1109/LRA.2022.3149031, provided by the authors.

Digital Object Identifier 10.1109/LRA.2022.3149031

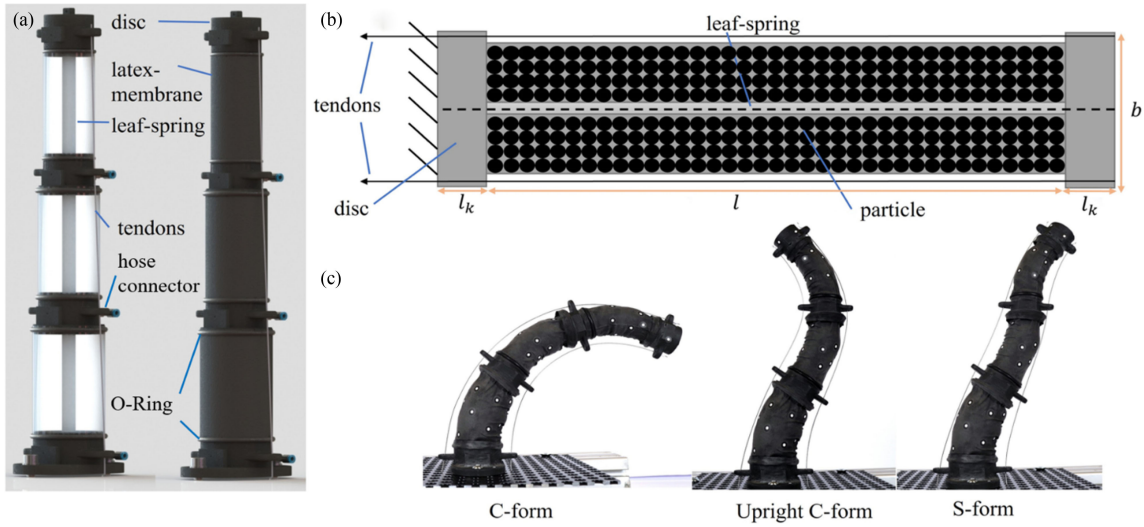

Fig. 1. Design of the soft continuum manipulator: (a) Structural view without particles and transparent covering (left) and real black covering (right), (b) Internal structure of a segment with dimensions, (c) Defined target shapes.

shape [15]. Therefore, a wide variety of approaches for kinematic modeling of soft bodied continuum robotic structures and especially variable stiffness robotic structures exists [16]. The most adopted practice to describe the kinematics of a continuum robot is to assume the bending shape as a constant curvature (CC) provided in [17], [18]. In presence of gravity this assumption leads to divergence, therefore other exact models are needed. In [19] analytical models for small deformations under tendon actuation, own weight and external loading were analyzed with the that more conclusion advanced models are needed to calculate the great deflections under these conditions.

Typically used advanced models among others are Cosserat Rod [15], reduced-order models (ROM) [20], beam models [16] and variable curvature (VC) kinematics combined with elasticity theories, shape functions and finite element modeling [21].

Ongoing research on continuum robots provides several approaches for variable stiffness modeling with CC-kinematics, VC-kinematics, ROM-models and beam-models [16], [20], [22]–[24] also used in this paper.

Multibody simulations are used to represent large deformations. A distinction is made between rigid MBS, linear-elastic MBS and nonlinear-elastic MBS [25]. After analyzing different approaches and according to the findings in the literature [15], [18], a rigid MBS approach with rigid elements connected by torsion springs is used in the present work, because it is comparatively fast and nearly as accurate as linear elastic MBS for the shown manipulator. Due to the high complexity and computational time of particle simulations, the jamming effect for modeling the variable stiffness behavior is assumed here simplified as rigid bodies in the stiff state and linear elastic bodies in the soft state.

II. Design of the Manipulator

The arm consists of three variable stiff segments with a bending length of l 70 mm for each segment and is designed to perform motion in one plane. Structural views of the manipulator are shown in Fig. 1. To realize the variable stiffness, the principle of particle jamming with coffee powder filled in a latex cover (latex thickness: 0.25 mm) is used. The materials are used because coffee powder shows comparatively good stiffening capabilities (low weight, fast stiffness change, high stiffness ratio) [6] and thin latex coverings have the needed combination of high extensibility for dense packing of particles during jamming and durability [3]. The latex coverings are made using latex glue for sealing an overlapping area of 10 mm from a flat pattern rolled into a tubular shape. To couple the segments, 3D stereolithographic-printed discs with outer loops for tendon guidance and a height of $l_{\mathrm{k}} = 30$ mm are used. The discs are coupled to each other using leaf springs as a backbone. The springs prevent contraction of segments due to tendon pressure and force the segments to bend continuously. They are glued to the coupling elements and only allow bending in a plane. The leaf spring thickness decreases from the bottom to the top (0.5 mm; 0.35 mm; 0.25 mm) with decreasing diameter b of the segments (50 mm; 42.5 mm; 35 mm) for reasons of weight reduction and stability and a smaller lever arm at the tip. The tendons (steel wire ropes with diameter d = 0.75 mm) are guided from the bottom to the top and are only fixed at the top of the manipulator.

In order to be able to position the segments independently, variable stiffness is used. For this purpose, any segment is switched soft and can be moved due to the tendons attached to the top of the manipulator and can be pulled by stepper motors at the bottom. The deformed shape can be held in place by particle jamming while the soft segments can be deformed. A vacuum pump connected to each segment with valves, tubes and hose connectors allows evacuation and refilling of air. O-ring seals ensure the required air tightness with the O-rings pressing from the outside onto the latex cover and into a corresponding groove, also for fixation. A cotton filter on each segment prevents particle leakage during air evacuation. The powder filled segments can

feature two conditions: a soft/compliant (vacuum pump off) and a stiff one (vacuum pump on).

III. Modeling of the Manipulator

Previous research has already investigated the comparison of different methods for the simulation of continuum robots with variable stiffness [15], [16], [18]. In analogy, a rigid MBS model, also called lumped parameter model [20], and a linear-elastic MBS model [16] were investigated in advance for their suitability to simulate the presented structure. The results confirmed the findings presented in the literature that the rigid MBS model requires significantly lower computation times, whereas the linear-elastic MBS model is a little more accurate. Both approaches provided similarly accurate values for our manipulator. For this reason, the rigid MBS approach will be used for the kinematic simulation of the structure in the further work [15], [18].

In a first step, the simulation is performed in the absence of gravity and compared with a CC kinematic calculation, precisely described in [17], to include in the study a widely used and highly simplified method, which consequently requires less computation time. In the CC calculation, it is assumed that each segment is bent by the tendons by pure bending as an arc of constant curvature neglecting gravity, in terms of segment position and pulled tendon length. In a second step, the simulation using the rigid MBS model is carried out in presence of gravity in order to validate it with experimentally determined results of the real system.

A. Conditions and Assumptions

To investigate the kinematic model approaches at different conditions, three shapes shown in Fig. 1 were defined: C-form, upright C-form, and S-form. Each shape is defined by a bending angle of each segment equal to 36°. The three shapes were chosen so that the number of bending points gradually increases starting from the C-shape with a bending point (sequence: C-, upright C- and S-shape) to present the independent motion of the segments and to investigate the changing influence of gravity in the model caused by varying the direction of bending of the segments.

In the modeling of the manipulator, we define the two states "soft" and "stiff" of the segments. The deformation of each segment is performed by the tendons in the soft state. In the models, we first assume that the powder and latex membrane do not affect the bending curvature and stiffness. We therefore consider the case where only the leaf spring (backbone) is relevant for the stiffness and bending shape in the soft state. It is assumed that the stiff switched segments and discs can be modelled as rigid bodies.

Further assumptions are the inextensibility of the tendons, that the movement of the segments takes place only in one plane and that the leaf spring behaves ideally linear elastic.

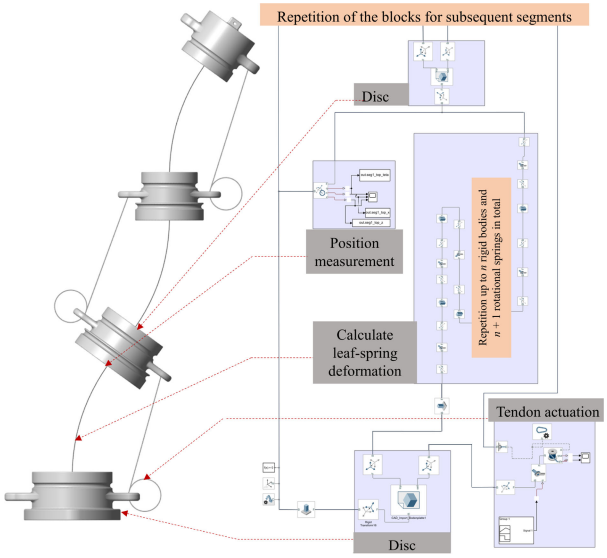

Fig. 2. Simulative visualization of the S-shape in *MATLAB* (left) and associated structure of the simulation model in block notation (right).

B. Building of the Simulation Model

To perform the kinematic simulation of the manipulator, a model was created in MATLAB Simulink using the Simscape Multibody package, in which the structural simulation using rigid MBS was implemented. The relevant section of the model is shown in Fig. 2.

Since the bending of the segments is initiated by only one tendon while the antagonistic tendon remains relaxed, the antagonistic tendon is not modeled to reduce the calculation time. Based on the assumption that the segments switched stiff can be modeled as rigid bodies, the tendons were placed at every segment, although in the real system they were only fixed at the top of the last segment. This reduces errors due to unstable tendon routing problems, twisting of tendons and tendon vibration. The three shapes of the model can be reached by changing the side of the tendons of each segment. For example, the C-form has all tendons on the right side while at the S-form the side alternates. The tendons were attached at the tendon guides of the discs.

For the rigid MBS model n discrete rigid bodies were coupled with $n + 1$ revolute joints with integrated rotational spring connection to represent the continuous bending of the segment (s. Fig. 2 block "Calculate leaf-spring deformation"). So, the springs are placed into series connection. Due to the assumption that the stiffness of a soft segment is equal to the stiffness of the leaf spring, the coupled rotational springs need to have the same stiffness combined. Based on this setup, the combined stiffness of the leaf spring c_ϕ has to be calculated using an Euler-Bernoulli beam differential equation to obtain the equivalent stiffness $c_{\phi i}$ for the $n + 1$ rotational springs. The angle of rotation ϕ at the end of the leaf-spring is expressed in (1) by beam theory with the Moment M, the moment of inertia I in (2), the length of the leaf-spring l and the Young's modulus E. Coupled with the rotational spring, which links angle of rotation, moment, and stiffness, it is possible to generate (3) for the combined stiffness

TABLE I
GEOMETRICAL AND MECHANICAL DATA OF THE LEAF SPRING

Young's modulus E	$200 \cdot 10^9$ N/m^2
Poisson's ratio ν	0.3
Leaf spring thickness t_1	0.00050 m
Leaf spring thickness t_2	0.00035 m
Leaf spring thickness t_3	0.00025 m
Leaf spring width b_f	0.01270 m
Leaf spring length l	0.07000 m

of the leaf spring. The series connection of rotational springs can be expressed with (2), (4) and (5) and the mechanical data, shown in Table I. The length of each *n* body is $l_n = l/n$.

$$\phi = \frac{M \cdot l}{E \cdot I} = \frac{M}{c_\phi} \tag{1}$$

$$I = \frac{b \cdot t_i^3}{12} \tag{2}$$

$$C_\phi = \frac{E \cdot I}{l} \tag{3}$$

$$\frac{1}{C_\phi} = \sum_{i=1}^{n+1} \frac{1}{C\phi \mathrm{i}} \tag{4}$$

$$c_{\phi i} = c_\phi \ \ (n+1) = \frac{E \cdot I}{l} \ \ (n+1) \tag{5}$$

Since with increasing number of elements a higher accuracy is achieved, but the calculation time increases, a suitable number of elements has to be found. For this purpose, a convergence analysis was performed with respect to the change of the bending angle when increasing the number of elements, with the aim of achieving a relative error of less than 0.1% between *n* and $n+1$ elements. The tendons were pulled to a constant length for all convergence steps.

As a result of the convergence analysis, we use 12 rigid bodies and 13 rotational springs as converged numbers. With Table I and (5) it is possible to calculate the stiffness $c_{\phi i}$ of the rotational springs in all three segments. For the first segment, this results in a value of 4.91 Nm/rad, for the second 1.69 Nm/rad and for the third 0.61 Nm/rad.

C. Simulation

The following analyses were performed in a transient study with 10 seconds of running time using a Backward Euler solver with a consistency tolerance of 10^{-9} as default value. The input parameter of the simulation is the corresponding pulled tendon length to achieve a bending angle of 36°. As output parameter *Simscape* calculates the position of calculation points. We defined our eight calculation points at the top and bottom of each disc shown as black dots in the middle plot in Fig. 5. At these specific points we compared the results in position for planar motion and pulled tendon length of the analytical CC-kinematic and the rigid MBS model in absence of gravity. Even though the model is dynamic, here we only study the static deviation at the end of the deformation process.

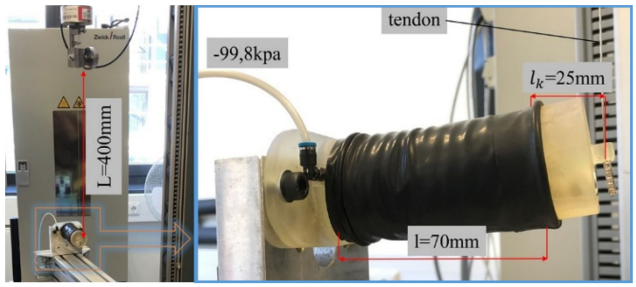

Fig. 3. Experimental setup for stiffness characterization.

In order to be able to model the behavior of the switchability of the stiffness in the simulation process, all three segments were first assumed to be ideally stiff. Starting from the bottom up, only the corresponding segment was discretized as described above while the other two were still defined as stiff and the position adjustment was calculated up to an angle of 36°. The results were exported in each case and served as a starting point for the next simulation step for the following segment. With this method it is possible to simulate the shape setting of the real system using the adaptive stiffness of the structure

IV. EXPERIMENTAL VALIDATION

A. Stiffness Characterization

To verify the assumption that soft segments can be characterized by the leaf spring alone, a bending stiffness analysis of the middle segment of the manipulator was performed, since the deformation of the middle segment shows the largest deviations between simulation model and experimental validation. For this purpose force-displacement curves were measured in a tensile-compression testing machine from *ZwickRoell*. As shown in Fig. 3, the segment was placed and fixed horizontally in the testing machine and deformed at the free tip using a tendon that is loaded vertically in tension to initiate bending of the segment. The tendon was connected to a load cell and crosshead so that the forces and displacements can be detected via load cell and crosshead travel. Pulling prevents pre-forming of the soft state due to gravity and enables calibration of the system to eliminate the weight force. Mounting the cable at a height of 400 mm reduces the force generated in the longitudinal direction of the segment and allows almost pure bending.

In order to show possible settlings or memory effects, the analysis was performed three times in a row in the same direction up to a vertical displacement of 10 mm. The distance-regulated measuring interval was 0.01 mm and the deformation speed was 0.1 mm/s.

As shown in Fig. 4, although the segment exhibits a nearly linear behavior in the soft state, the curves deviate slightly from each other due to the restructuring of the powder during the bending process. Therefore, by forming a linear regression function over all three measurements, the effective bending stiffness k was calculated as the slope of this regression line. The bending stiffness for the soft state determined this way is $k_{\mathrm{soft}} = 7.2 \cdot 10^{-2}$ N/mm over the entire displacement range.

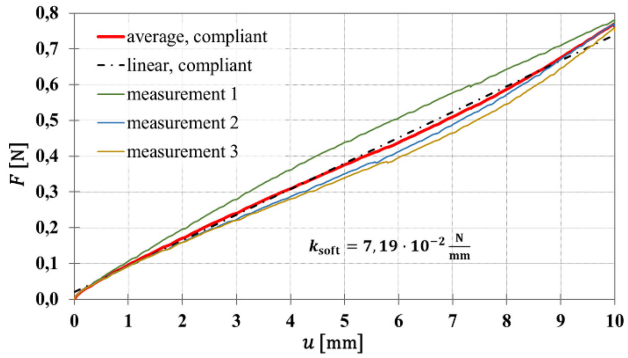

Fig. 4. Force-displacement plots of the middle segment in the soft state.

To calculate the bending stiffness of the segment in form of *EI* the differential Eq. (6) of the bending line is used, with the displacement u, direction z, bending moment M_b, Young's modulus E and moment of inertia I. In combination with Eq. (7) for the experimental segment stiffness k, it is possible to eliminate the resulting variables of force F and displacement u in the resulting Equation of the bending line. This leads to (8) and the required material properties *EI*.

$$u''(z) = -\frac{M_\mathrm{b}(z)}{EI} \tag{6}$$

$$k = \frac{F}{u} = 7.2 \cdot 10^{-2}\ \mathrm{N/mm} \tag{7}$$

$$EI = k \cdot \left({l_k}^2 l + l_k l^2 + \frac{1}{3} l^3 \right) = 0.0202\ \mathrm{N \cdot m^2} \tag{8}$$

With Eqs. (5) and (8), the real spring stiffness for the simulation in the soft state can be calculated to 3.75 Nm/rad. Compared with the value of 1.69 Nm/rad determined by calculating the leaf spring stiffness only, there is a relative error of 55%. Hence the simulation value of the spring stiffness for the middle segment is adapted with the new real value to improve the accuracy of the model.

B. Position Measurement of Target Shapes

To measure the position of the segments in the three defined target shapes and to detect the needed tendon length to reach the bending angle of 36°, an optical picture-based 3D scanner named *GOM Atos triple scan* with the analysis-software *GOM Inspect* was used.

First, the manipulator was positioned completely upright and a first reference picture was taken with all segments turned stiff. Then, the specific target shape (C-form, upright C-form, or S-form) was set by softening only one segment at the time and pulling the tendons accordingly to achieve the angle of 36°. This was done in the same way as the simulation, step by step for each segment from bottom to top. The pulling lengths of the tendons required for the angular adjustment were determined in preliminary tests and marked accordingly in order to be able to set them correctly by hand in the measurements. The manipulator was scanned from 20 different perspectives for each target shape. Reference points on the surface of the latex membrane enabled the software to recognize the different perspectives and combine them into a 3D mesh. With the *GOM Inspect* software, it is possible to determine the bending angle, the required tendon length and the position of the segments from the mesh (see Fig. 5 above plots). The red points marked in the left plot in Fig. 5 were defined as fixed reference points for the position measurement. To compare the measurements with the simulation results, the positions of the points at the top and bottom of the discs corresponding to those of the simulation were determined by transformation.

V. Experimental Results

In view to compare the experimental values of the three shapes determined with the optical measurement system with the analytical solution (CC-kinematics) and with the kinematic simulation (rigid MBS), all results are shown in a diagram per target shape in Fig. 5. It can be seen that both calculation methods give similar results to the measurement in absence of gravity. The error here is less than 2%. The small error, despite the absence of gravity in the calculations, could be explained by the fact that it was assumed that the powder and the membrane have no influence on the stiffness and the bending curve in the soft state. Even if the results of the first calculation step without gravity seem to represent the system sufficiently, i.e., the much simpler CC calculation could also be used, this only applies to the very specific configuration of the system investigated without applied forces and is not transferable. However, in order to ensure transferability and to be able to design the calculation methodology as generally as possible, calculations including gravity must be carried out in the second step.

In the presence of gravity, the position error for the rigid MBS increases to 22% for the C-form, confirming the assumption that powder and membrane contribute significantly to the segment stiffness in the soft state and further stabilize it. For this reason, the own weight deformation is larger in the simulation than in the measurements. The highest position error under gravity occurs for the C-Form in the second segment due to the larger arms of lever from the center of masses. To reduce the position error, the stiffness of the second segment was calculated from force-displacement measurements and implemented into the simulation model, as described in Section IV. A. *Stiffness Characterization*. Implementing this corrected stiffness into the rigid MBS model leads to the purple squares in the C-form in Fig. 5. Using the characterized stiffness of the middle segment in soft state, it was possible to reduce the position error to 3%. Nevertheless, the error is greater than for the calculations without gravity, since only the stiffness of the second segment was measured and implemented. To obtain an accurate calculation of the position under gravity, a stiffness characterization of all three segments is required. The upright C-form and S-form have lower errors under gravity because they are more upright, so the masses of the following segments have smaller arms of lever. Hence the simulation with corrected stiffness is only shown for the C-form in Fig. 5.

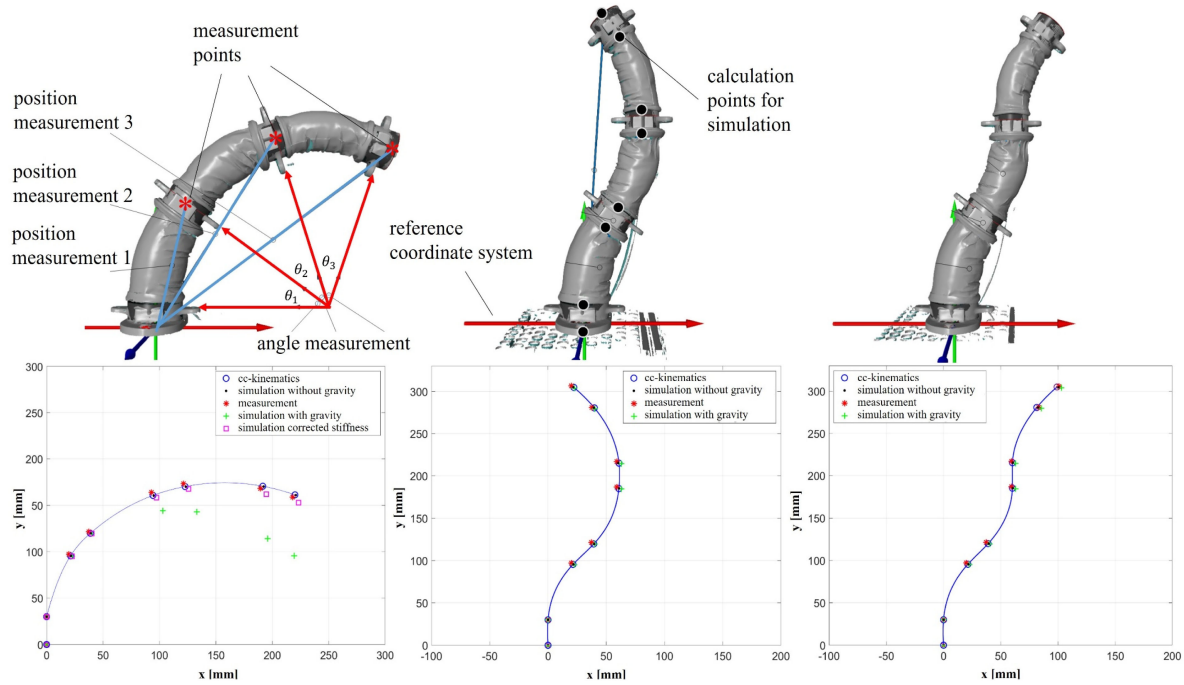

Fig. 5. Position measurements visualised and evaluated in *GOM Inspect* (top) and associated diagrams with experimental and simulation data (bottom).

VI. Conclusion

The design of a robot structure with variable stiffness through the use of particle jamming was demonstrated. Using the example of a 3-segment robot arm, it was shown that by using this structure, combined with only two tendon actuators, various shapes can be realized by planar deformation. The number of actuators required could be significantly reduced compared to existing systems. This demonstrates that by using structural elements with variable stiffness in combination with tendon actuators, it's possible to develop underactuated systems that can realize complex shapes.

It has been demonstrated that a planar deformation of the 3-segment structure can be calculated using a kinematic forward model based on rigid MBS, which is capable of large deflections with tendon actuators for underactuated soft continuum robots with variable stiffness properties. The model is able to calculate the position of the segments of all three defined target shapes with an error $< 2\%$ in absence of gravity. For the rigid MBS model, rotational springs were connected in series and their stiffness was calculated using beam theory and the linear spring equation. In a first assumption, only the leaf spring was considered for the stiffness calculation. The experimental validation with an optical 3D scanner showed that this assumption leads to a position error of 22% when gravity is included. Therefore the linearized stiffness for the soft state of the second segment was calculated from force-displacement measurements and implemented into the model. With the corrected stiffness it was possible to lower the error to 3% for the rigid MBS model in presence of gravity. The remaining error occurs because only the stiffness for the soft state of the second segment got measured and linearized.

For the upcoming work it is necessary to determine the stiffness of all three segments in soft and stiff state. Both states of stiffness for all segments need to be implemented into the model to improve the position calculations. Using only the measured and linearized stiffness will lead to a computationally fast and reasonably accurate kinematic model, when the deformations in stiff state do not exceed linear elastic material behavior. But if there are larger deformations and forces, also a non-linear material behavior of the stiff segments can occur. Therefore it could be useful to implement piecewise and deformation-dependent stiffness values for both states out of the measured values.

Further research will focus on measuring and implementing stiffness values for all segments and states, extending planar motion to 3D motion, as well as adding sensors to the robotic manipulator and building a control system for underactuated soft continuum robots with variable stiffness structures using the developed simulation model.

References

[1] D. Rus and M. T. Tolley, "Design, fabrication and control of soft robots," *Nature*, vol. 521, no. 7553, pp. 467–475, 2015.
[2] D. Trivedi, C. D. Rahn, and W. M. Kier, "Soft robotics: Biological inspiration, state of the art, and future research," *Appl. Bionics Biomech., vol.*, vol. 5, no. 3, pp. 99–117, 2008.
[3] M. Manti, V. Cacucciolo, and M. Cianchetti, "Stiffening in soft robotics: A review of the state of the art," *IEEE Robot. Automat. Mag.*, vol. 23, no. 3, pp. 93–106, Sep. 2016.
[4] L. Wang *et al.*, "Controllable and reversible tuning of material rigidity for robot applications," *Mater. Today*, vol. 21, no. 5, pp. 563–576, 2018.
[5] A. B. Clark and N. Rojas, "Assessing the performance of variable stiffness continuum structures of large diameter," *IEEE Robot. Automat. Lett.*, vol. 4, no. 3, pp. 2455–2462, Jul. 2019.

[6] N. G. Cheng *et al.*, "Design and analysis of a robust, low-cost, highly articulated manipulator enabled by jamming of granular media," in *Proc. IEEE Int. Conf. Robot. Automat.*, pp. 4328–4333, May 2012.

[7] W. R. Wockenfuß, L. Weisheit, and S. Rieß, "Strukturkomponenten mit schaltbarer steifigkeit für die soft-robotik/structural components with adjustable stiffness for soft robotics," *Konstruktion*, vol. 73, no. 5, pp. 61–66, 2021.

[8] M. Cianchetti, T. Ranzani, G. Gerboni, I. De Falco, C. Laschi, and A. Menciassi, "STIFF-FLOP surgical manipulator: Mechanical design and experimental characterization of the single module," in *Proc. IEEE/RSJ IROS Int. Conf. Intell. Robots Syst.*, Nov. 2013, pp. 3576–3581.

[9] A. Stilli, H. A. Wurdemann, and K. Althoefer, "Shrinkable, stiffness-controllable soft manipulator based on a bio-inspired antagonistic actuation principle," in *Proc. IEEE/RSJ IROS Int. Conf. Intell. Robots Syst.*, Sep. 2014, pp. 2476–2481.

[10] V. Falkenhahn, A. Hildebrandt, and R. Neumann, "Dynamic control of the bionic handling assistant," *IEEE/ASME Trans. Mechatronics*, vol. 22, no. 1, pp. 6–17, Sep. 2017.

[11] D. Ji, T. H. Kang, and S. Shim, "Wire-driven flexible manipulator with constrained spherical joints for minimally invasive surgery," *Int. J. Comput. Assist. Radiol. Surg.*, vol. 14, no. 8, pp. 1365–1377, 2019.

[12] Y. Kim, S. S. Cheng, and J. P. Desai, "Active stiffness tuning of a Spring-based continuum robot for MRI-guided neurosurgery," *IEEE Trans. Robot.*, vol. 34, no. 1, pp. 18–28, Oct. 2018.

[13] M. Selvaggio *et al.*, "The MUSHA underactuated hand for robot-aided minimally invasive surgery," *Int. J. Med. Robot. Comput. Assist. Surg.*, vol. 15, no. 3, 2019, Art. no. e1981.

[14] T. Hassan *et al.*, "Design and development of a bio-inspired, under-actuated soft gripper," in *Proc. 37th Annu. Int. Conf. IEEE Eng. Med. Biol. Soc.*, Aug. 2015, pp. 3619–3622.

[15] D. C. Rucker and R. J. Webster III, "Statics and dynamics of continuum robots with general tendon routing and external loading," *IEEE Trans. Robot.*, vol. 27, no. 6, pp. 1033–1044, Jul. 2011.

[16] S. H. Sadati *et al.*, "TMTDyn: A matlab package for modeling and control of hybrid rigid–continuum robots based on discretized lumped systems and reduced-order models," *Int. J. Robot. Res.*, vol. 40, no. 1, pp. 296–347, 2021.

[17] A. K. Mishra, A. Mondini, E. Del Dottore, A. Sadeghi, F. Tramacere, and B. Mazzolai, "Modular continuum manipulator: Analysis and characterization of its basic module," *Biomimetics*, vol. 3, no. 1, 2018.

[18] M. T. Chikhaoui, S. Lilge, S. Kleinschmidt, and J. Burgner-Kahrs, "Comparison of modeling approaches for a tendon actuated continuum robot with three extensible segments," *IEEE Robot. Automat. Lett.*, vol. 4, no. 2, pp. 989–996, Jan. 2019.

[19] K. Oliver-Butler, J. Till, and C. Rucker, "Continuum robot stiffness under external loads and prescribed tendon displacements," *IEEE Trans. Robot.*, vol. 35, no. 2, pp. 403–419, Jan. 2019.

[20] S. Sadati *et al.*, "Reduced order vs. discretized lumped system models with absolute and relative states for continuum manipulators," in *Proc. Robot. Sci. Syst. Conf.*, 2019, pp. 1–10.

[21] S. Grazioso, G. Di Gironimo, and B. Siciliano, "A geometrically exact model for soft continuum robots: The finite element deformation space formulation," *Soft Robot.*, vol. 6, no. 6, pp. 790–811, 2019.

[22] S. H. Sadati, S. Zschaler, and C. Bergeles, "A matlab-internal DSL for modelling hybrid rigid-continuum robots with TMTDyn," in *Proc. ACM/IEEE 22nd Int. Conf. Model Driven Eng. Languages Syst. Companion (MODELS-C)*, Sep. 2019, pp. 559–567.

[23] S. M. H. Sadati *et al.*, "A geometry deformation model for braided continuum manipulators," *Front. Robot. AI*, vol. 4, 2017.

[24] S. M. H. Sadati *et al.*, "Stiffness imaging with a continuum appendage: Real-time shape and tip force estimation from base load readings," *IEEE Robot. Automat. Lett.*, vol. 5, no. 2, pp. 2824–2831, Feb. 2020.

[25] O. A. Bauchau, "Flexible multibody dynamics," in *Solid Mechanics Applications*, Dordrecht, Heidelberg London New York: Springer, 2011, vol. 176, pp. 481–507.